Composite Structures 92 (2010) 835–843

Contents lists available at ScienceDirect

Composite Structures

journal homepage: www.elsevier.com/locate/compstruct

Interlaminar shear stresses around an internal part-through hole in a stretched laminated composite plate

Reaz A. Chaudhuri [a,*], Paul Seide [b]

[a] Department of Materials Science & Engineering, University of Utah, 122 S. Central Campus Drive, Room 304, Salt Lake City, UT 84112-0560, USA
[b] Department of Civil & Environmental Engineering, University of Southern California, 3620 S. Vermont Avenue, KAP 210, Los Angeles, CA 90089-2531, USA

ARTICLE INFO

Article history:
Available online 31 August 2009

Keywords:
Composite laminate
Internal or embedded circular cylindrical hole
Bi-material wedge singularity
Interfacial compatibility
Boundary layer effect
Interlaminar shear stress

ABSTRACT

The equilibrium/compatibility method, which is a semi-analytical post-processing method, is employed for computation of hitherto unavailable through-thickness variation of interlaminar (transverse) shear stresses in the vicinity of the bi-layer interface circumferential re-entrant corner line of an internal part-through circular cylindrical hole weakening an edge-loaded laminated composite plate. A C^0-type triangular composite plate element, based on the assumptions of transverse inextensibility and layer-wise constant shear-angle theory (LCST), is utilized to first compute the in-plane stresses and layer-wise through-thickness average interlaminar shear stresses, which serve as the starting point for computation of through-thickness distribution of interlaminar shear stresses in the vicinity of the bi-layer interface circumferential re-entrant corner line of the part-through hole. The same stresses computed by the conventional equilibrium method (EM) are, in contrast, in serious errors in the presence of the bi-layer interface circumferential re-entrant corner line singularity arising out of the internal part-through hole, and are found to violate the interfacial compatibility condition. The computed interlaminar shear stress can vary from negative to positive through the thickness of a cross-ply plate in the neighborhood of this kind of stress singularity.

1. Introduction

Advanced composite materials (e.g., graphite/epoxy, boron/epoxy, Kevlar/epoxy, graphite/PEEK, etc.) are replacing metallic alloys at an accelerated pace in the fabrication of structural components in both military (e.g., stealth fighter F-117A Nighthawk and B-2 bomber) and commercial (e.g., the forthcoming Boeing 787 Dreamliner) airplanes. This is because of many beneficial properties, such as higher strength-to-weight ratios, longer in-plane fatigue (including sonic fatigue) life, better stealth characteristics, enhanced corrosion resistance, and most significantly, the possibility of optimal design through the variation of stacking pattern, fiber orientation, and so forth, known as composite tailoring. These advantages notwithstanding, polymeric composite plate type structures are highly prone to transverse (or interlaminar) shear related fatigue failures, as a result of the matrix material being of relatively low shearing stiffness as compared to the longitudinal stiffness of the fibers. A reliable prediction of the response of these laminated plates must account for transverse (or interlaminar) shear deformation.

The issues concerning the weakening effects of through-thickness holes in both homogeneous isotropic as well as laminated composite plates are well understood in the literature [1–5]. In contrast, the problems of stress concentration in the vicinity of internal part-through holes weakening both homogeneous as well as laminated plates have till recently remained a virgin territory [6–9]. Embedded part-through holes are more realistic representations of internal flaws and damages. For example, part of the material inside one or more layers may be missing as a result of faulty manufacturing techniques, which may propagate during service with catastrophic consequences. The fact that these internal holes can cause severe cross-sectional warping resulting in interlaminar or transverse strains and stresses even in a stretched/compressed plate, and as a result may initiate shear crippling failure in compression or shear/delamination failure in tension in advanced composite laminates is a matter of serious concern to structural designers. Additionally, these interlaminar stresses in the neighborhood of such a hole in a stretched homogeneous isotropic as well as laminated anisotropic plate vary through the thickness, which brings three-dimensional effect even in a thin plate weakened by such an embedded part-through hole [6–9]. Finally, the effect of stress singularity in the neighborhood of the bi-layer interface circumferential re-entrant corner line of the part-through internal hole weakening a laminated plate is also of serious concerns.

Although reasonably accurate (finite element based) post-processing type methods for determination of interlaminar or

* Corresponding author. Tel.: +1 801 581 6282; fax: +1 801 581 4816.
E-mail address: r.chaudhuri@utah.edu (R.A. Chaudhuri).

0263-8223/$ - see front matter © 2009 Elsevier Ltd. All rights reserved.
doi:10.1016/j.compstruct.2009.08.042

Nomenclature

a, b	length and width, respectively, of a rectangular laminated plate
$[B_j^{(i)}]$	strain-nodal displacement relation matrix for the jth triangular layer-element belonging to the ith layer
$[C^{(i)}]$, $[G^{(i)}]$	in-plane and transverse elastic stiffness matrices of the ith orthotropic lamina
$c_{jk}^{(i)}$	components of the elastic stiffness matrix of the ith orthotropic lamina
$[D_L]$	integrated (through thickness) elastic stiffness matrix
$\{d_j^{(i)}\}$	nodal displacement vector of the jth triangular layer-element belonging to the ith layer
$\bar{d}_i$	distance from the bottom (reference) surface
E_{11}, E_{22}	Young's moduli of an orthotropic lamina in the direction of fibers and normal to the fibers, respectively
$\{F_j\}$	consistent load vector of the jth composite plate element
g_α, g_β	first fundamental quantities for orthogonal curvilinear coordinates for a flat plate
G_{12}	in-plane shear modulus of an orthotropic lamina
G_{13}, G_{23}	transverse shear moduli of an orthotropic lamina
h	total depth of an internal part-through hole
$[K_j]$	stiffness matrix for the jth composite plate element
ℓ_α, ℓ_β	direction cosines of normal with respect to α and β coordinates, respectively
N	total number of layers or laminae
q	applied uniform tension at the edge of a plate
r, θ, z	polar cylindrical coordinates
r_0	radius of an internal part-through circular cylindrical hole
t_i, t	thickness of the ith lamina and laminated plate, respectively
U	strain energy of a laminated plate
$\overline{U}$	strain energy per unit area
$U_I^{(i)}$	strain energy due to intra-laminar stresses and strains of the ith layer
$U_S^{(i)}$	strain energy due to interlaminar (transverse) shear stresses and strains of the ith layer
u_i	in-plane components of the displacement vector, $i = \alpha, \beta$
W	potential due to external conservative forces
w	transverse displacement component (deflection) of a plate
x, y, z	Cartesian coordinates in the length, width and thickness directions of a laminated plate
α, β	in-plane (orthogonal) curvilinear coordinates
$\gamma_{\alpha\beta}^{(i)}$	in-plane (engineering) shearing strain at a point inside the ith layer
$\gamma_{\alpha z}^{(i)}$, $\gamma_{\beta z}^{(i)}$	transverse (engineering) shearing strains at a point inside the ith layer
Δ_j	reference surface area of the jth element
$\varepsilon_k^{(i)}$	in-plane normal strains at a point inside the ith layer; $k = \alpha, \beta$
ν_{12}, ν_{13}, ν_{23}	major Poisson's ratios of an orthotropic lamina
Π	total potential energy functional
$\bar{\theta}_i$	fiber orientation angle of the ith lamina
$\bar{\sigma}_{nn}^{(i)}(z)$, $\bar{\tau}_{n\Gamma}^{(i)}(z)$, $\bar{\tau}_{nz}^{(i)}(z)$	applied stresses at a boundary distributed through the thickness of the ith layer
$\{\phi\}$	shape functions

transverse shear stresses in homogeneous and laminated plates and shells have been developed in the 1980's [10–15], a detailed review of the literature reveals that till recently the issue of determination of transverse shear stresses in the vicinity of an internal (or embedded) part-through hole weakening a plate subjected to all-round tension has remained unaddressed in the literature [16,17]. Majority of the finite element based post-processing approaches employ equilibrium equations of three-dimensional elasticity theory, referred to here as equilibrium method, the only exceptions being Chaudhuri and Seide [13], and Chaudhuri [14]. These authors have introduced a semi-analytical post-processing method, termed equilibrium/compatibility method, wherein both the equilibrium equations as well as interfacial compatibility conditions are satisfied in the point-wise sense. The latter approach has recently been employed for computation of hitherto unavailable through-thickness variation of transverse shear stresses in the vicinity of the circumferential re-entrant corner lines of internal part-through circular and elliptical cylindrical holes weakening edge-loaded isotropic plates [16,17]. A detailed review of the literature, however, reveals that the determination of interlaminar shear stresses in the vicinity of an internal (or embedded) part-through hole weakening a laminated anisotropic plate, subjected to all-round tension, has still remained unaddressed in the literature. The primary objective of the present investigation is to fill this important gap. In what follows, a curvilinear triangular element, based on the assumptions of transverse inextensibility and layer-wise constant shear angle (LCST), is employed as a starting point to determine the through-thickness distribution of interlaminar or transverse shear stresses in the vicinity of an embedded circular part-through hole, weakening a general cross-ply plate, using a method that satisfies the equilibrium as well as interfacial compatibility in the point-wise sense. In this connection, it may be noted that the stress singularity, in the neighborhood of the bi-layer interface circumferential re-entrant corner line of the internal part-through hole, is that of a bi-material wedge type singularity [18,19] of which the well-known free-edge stress singularity [20–23] is a special case.

2. Theoretical background and finite element formulation

Fig. 1 shows an N-layer laminated composite triangular element with its bottom surface designated as the reference surface. The curvilinear triangular element is ideally suited for analysis of a laminated anisotropic plate weakened by a part-through hole of arbitrary geometry (e.g., circular, elliptical, etc.). The small deformation of such weakened plates [6–8] can be analyzed using a finite element formulated on the basis of assumptions of transverse inextensibility and layer-wise constant shear angle [24–26]. The special case of a moderately thick plate weakened by a through hole [4] can be analyzed by a finite element formulation based on the Mindlin hypothesis [27,28].

The local or element coordinates are denoted by α, β and z, while the corresponding global or plate coordinates are represented by x, y and z. The curvilinear coordinates for the special case of circular geometry are given by

$$\alpha = r, \quad \beta = \theta, \quad g_\alpha = 1, \quad g_\beta = r. \tag{1}$$

The distribution of displacement components for the ith layer, based on the above assumptions, can be written as follows [24–26]:

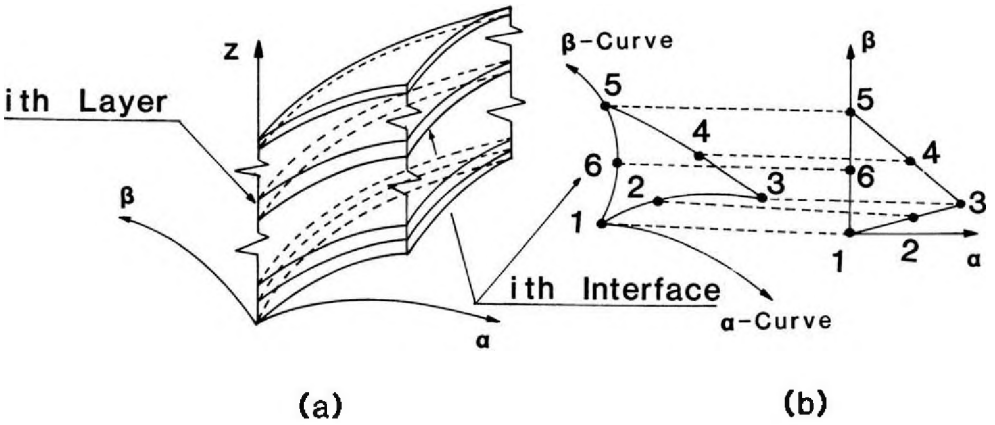

Fig. 1. (a) Triangular composite element with curved boundary, (b) mapping of its interface onto a straight-sided quadratic triangular element in the curvilinear coordinate plane.

$$u_m^{(i)}(z) = \left(1 - \frac{z}{t_i}\right)\bar{u}_m^{(i)} + \frac{z}{t_i}\bar{u}_m^{(i+1)}, \quad m = \alpha, \beta \tag{2a}$$

$$w^{(i)}(z) = w. \tag{2b}$$

α and β are general curvilinear coordinates in the plane of the plate. z is the transverse coordinate local to the ith layer, and is measured from its bottom surface. Based on the above-mentioned kinematic approximations given by Eq. (2), the in-plane strains at a point inside a layer can be expressed in terms of their counterparts at the top and bottom surfaces of the same layer as follows:

$$\{\varepsilon^{(i)}(z)\} = \left[\left[A_b^{(i)}(z)\right] \quad \left[A_t^{(i)}(z)\right]\right] \begin{Bmatrix} \{\bar{\varepsilon}^{(i)}\} \\ \{\bar{\varepsilon}^{(i+1)}\} \end{Bmatrix}, \tag{3}$$

in which $\left[A_b^{(i)}(z)\right]$ and $\left[A_t^{(i)}(z)\right]$ are as given by Eqs. (A2a) and (A2b) in the Appendix, while

$$\{\varepsilon^{(i)}(z)\}^T = \left\{\varepsilon_\alpha^{(i)}(z),\ \varepsilon_\beta^{(i)}(z),\ \gamma_{\alpha\beta}^{(i)}(z)\right\}, \quad i = 1, \ldots, N, \tag{4a}$$

and

$$\{\bar{\varepsilon}^{(i)}\}^T = \left\{\bar{\varepsilon}_\alpha^{(i)},\ \bar{\varepsilon}_\beta^{(i)},\ \bar{\gamma}_{\alpha\beta}^{(i)}\right\}, \quad i = 1, \ldots, N+1, \tag{4b}$$

where $\bar{\varepsilon}_\alpha^{(i)}$, $\bar{\varepsilon}_\beta^{(i)}$ and $\bar{\gamma}_{\alpha\beta}^{(i)}$ represent the in-plane strains at the ith interface.

The interlaminar or transverse shear strains in the ith lamina are given by

$$\{\bar{\gamma}^{(i)}\}^T = \left\{\bar{\gamma}_{\alpha z}^{(i)},\ \bar{\gamma}_{\beta z}^{(i)}\right\}, \quad i = 1, \ldots, N \tag{5}$$

The transverse shear stresses and strains are constant through thickness of a layer by virtue of the aforementioned assumptions, and can, therefore, be assumed to be the through-layer-thickness averages of the actual transverse shear stresses and strains.

The in-plane strains, $\bar{\varepsilon}_\alpha^{(i)}$, $\bar{\varepsilon}_\beta^{(i)}$ and $\bar{\gamma}_{\alpha\beta}^{(i)}$, at the ith interface are given by

$$\bar{\varepsilon}_\alpha^{(i)} = \frac{1}{g_\alpha}\left(\bar{u}_{\alpha,\alpha}^{(i)} + \frac{\bar{u}_\beta^{(i)}}{g_\beta} g_{\alpha,\beta}\right), \tag{6a}$$

$$\bar{\varepsilon}_\beta^{(i)} = \frac{1}{g_\beta}\left(\bar{u}_{\beta,\beta}^{(i)} + \frac{\bar{u}_\alpha^{(i)}}{g_\alpha} g_{\beta,\alpha}\right), \tag{6b}$$

$$\bar{\gamma}_{\alpha\beta}^{(i)} = \frac{1}{g_\beta}\left(\bar{u}_{\alpha,\beta}^{(i)} - \frac{\bar{u}_\alpha^{(i)}}{g_\alpha} g_{\beta,\alpha}\right) + \frac{1}{g_\alpha}\left(\bar{u}_{\beta,\alpha}^{(i)} - \frac{\bar{u}_\beta^{(i)}}{g_\beta} g_{\alpha,\beta}\right), \tag{6c}$$

while the average transverse shear strains in the ith layer are given as follows:

$$\bar{\gamma}_{jz}^{(i)} = \frac{1}{g_\alpha} w_{,j} + \frac{1}{t_i}\left(\bar{u}_j^{(i+1)} - \bar{u}_j^{(i)}\right), \quad j = \alpha, \beta \tag{7}$$

The assumed displacement potential energy based finite element equations are available elsewhere [6–8], and will not be repeated here in the interest of brevity of presentation. As a first step, the boundary of a circular hole is modeled using straight-sided version of the present triangular element, which behaves more like a subparametric element, while the curvilinear triangular element would behave similar to a superparametric or isoparametric element. In the case of a subparametric finite element, the error in strain energy due to domain approximation, $O(h^3)$, dominates its counterpart due to usual finite element approximation, $O(h^4)$, as suggested by Berger's lemma [29]. Once the nodal displacements are computed using the finite element method, the layer-element stresses can be obtained using the following relation [13]:

$$\left\{\sigma^{(i)}(z)\right\}^T = \left[C^{(i)}\right]\left[A^{(i)}(z)\right]\left[B_j^{(i)}\right]\left\{d_j^{(i)}\right\}, \tag{8}$$

where

$$\left\{\sigma^{(i)}(z)\right\}^T = \left\{\sigma_x^{(i)}(z),\ \sigma_y^{(i)}(z),\ \tau_{xy}^{(i)}(z),\ \bar{\tau}_{xz}^{(i)},\ \bar{\tau}_{yz}^{(i)}\right\}, \tag{9}$$

and $\left[C^{(i)}\right]$, $\left[A^{(i)}(z)\right]$, $\left[B_j^{(i)}\right]$ and $\left\{d_j^{(i)}\right\}$ are given in the Appendix.

3. Determination of interlaminar shear stresses using the equilibrium/compatibility method

The assumptions of layer-wise constant shear-angle theory (LCST) implies parabolic variation of interlaminar (transverse) shear strains and stresses through the thickness of a layer. This implies, for example, that $\tau_{xz}^{(i)}(z)$ is of the form [13,14]:

$$\tau_{xz}^{(i)}(z) = N_1(z)\bar{f}_1^{(i)} + N_2(z)\bar{f}_2^{(i)} + N_3(z)\bar{f}_3^{(i)}, \tag{10}$$

where $\bar{f}_1^{(i)}$, $\bar{f}_2^{(i)}$ and $\bar{f}_3^{(i)}$ represent $\tau_{xz}^{(i)}(z)$ at the bottom, middle and top surface, respectively, of the ith layer. $N_1(z)$, $N_2(z)$ and $N_3(z)$ are one-dimensional quadratic shape functions, defined by

$$N_1(z) = 1 - \frac{3z}{t_i} + \frac{2z^2}{t_i^2}, \quad N_2(z) = \frac{4z}{t_i} - \frac{4z^2}{t_i^2}, \quad N_3(z) = -\frac{z}{t_i} + \frac{2z^2}{t_i^2}. \tag{11}$$

τ_{xz} distribution through the thickness of a N-layer laminate, therefore, requires $3N$ unknown parameters, which, in turn, ask for $3N$ equations. The present equilibrium/compatibility method supplies these equations, by (i) forcing τ_{xz} to vanish on the top and bottom

surfaces of the laminate (2 equations), (ii) satisfying continuity of τ_{xz} at each layer-interface ($N-1$ equations), (iii) identifying $\bar{\tau}_{xz}^{(i)}$, as computed by Eqs. (8) and (9) of Section 2 above, as the through-the-layer-thickness average of $\tau_{xz}^{(i)}(\mathbf{z})$ (N equations), and (iv) computing jump in $\tau_{xz,z}$ at each interface utilizing the first equation of equilibrium in terms of stresses ($N-1$ equations) [13].

Conditions (i) and (ii) above imply

$$\bar{f}_1^{(1)} = \bar{f}_3^{(N)} = 0, \tag{12}$$

$$\bar{f}_1^{(i)} = \bar{f}_3^{(i-1)}, \quad i = 2, \ldots, N. \tag{13}$$

Condition (iii) yields

$$\frac{1}{t_i}\int_0^{t_i} \tau_{xz}^{(i)}(z)\, dz = \begin{bmatrix} 0, & 0, & 0, & 0, & 0, & 0, & c_{44}^{(i)}, & c_{45}^{(i)} \end{bmatrix} \times \left[B_j^{(i)}\right] \left\{d_j^{(i)}\right\}, \quad \text{for } i = 1, \ldots, N \tag{14}$$

which, with the help of Eqs. (10)–(13), become

$$\left(\frac{1}{6}\bar{f}_1^{(i)} + \frac{2}{3}\bar{f}_2^{(i)} + \frac{1}{6}\bar{f}_3^{(i)}\right) = \begin{bmatrix} 0, & 0, & 0, & 0, & 0, & 0, & c_{44}^{(i)}, & c_{45}^{(i)} \end{bmatrix} \left[B_j^{(i)}\right] \left\{d_j^{(i)}\right\}, \quad \text{for } i = 2, \ldots, N-1 \tag{15a}$$

$$\left(\frac{2}{3}\bar{f}_2^{(1)} + \frac{1}{6}\bar{f}_3^{(1)}\right) = \begin{bmatrix} 0, & 0, & 0, & 0, & 0, & 0, & c_{44}^{(1)}, & c_{45}^{(1)} \end{bmatrix} \left[B_j^{(1)}\right] \left\{d_j^{(1)}\right\}, \tag{15b}$$

$$\left(\frac{1}{6}\bar{f}_3^{(N-1)} + \frac{2}{3}\bar{f}_2^{(N)}\right) = \begin{bmatrix} 0, & 0, & 0, & 0, & 0, & 0, & c_{44}^{(N)}, & c_{45}^{(N)} \end{bmatrix} \left[B_j^{(N)}\right] \left\{d_j^{(N)}\right\}. \tag{15c}$$

The left and right sides of the remaining $N-1$ equations are given by condition (iv) above, and are obtained by using Eqs. (10) and (11) and the first equation of equilibrium, respectively.

The jump at the $(i+1)$ th interface as computed using Eq. (10), is given as follows:

$$\begin{aligned} J_x^{(i+1)} &= \frac{\partial \tau_{xz}^{(i+1)}(0)}{\partial z} - \frac{\partial \tau_{xz}^{(i)}(t_i)}{\partial z} \\ &= \left[\frac{\partial N_1(z)}{\partial z}\bar{f}_3^{(i)} + \frac{\partial N_2(z)}{\partial z}\bar{f}_2^{(i+1)} + \frac{\partial N_3(z)}{\partial z}\bar{f}_3^{(i+1)}\right]_{z=0} \\ &\quad - \left[\frac{\partial N_1(z)}{\partial z}\bar{f}_3^{(i-1)} + \frac{\partial N_2(z)}{\partial z}\bar{f}_2^{(i)} + \frac{\partial N_3(z)}{\partial z}\bar{f}_3^{(i)}\right]_{z=t_i}, \end{aligned} \tag{16}$$

which, with the help of Eq. (11), becomes

$$J_x^{(i+1)} = -\frac{1}{t_i}\bar{f}_3^{(i-1)} + \frac{4}{t_i}\bar{f}_2^{(i)} - 3\left(\frac{1}{t_i} + \frac{1}{t_{i+1}}\right)\bar{f}_3^{(i)} + \frac{4}{t_{i+1}}\bar{f}_2^{(i+1)} - \frac{1}{t_{i+1}}\bar{f}_3^{(i+1)}, \quad \text{for } i = 2, \ldots, N-2 \tag{17a}$$

$$J_x^{(2)} = \frac{4}{t_1}\bar{f}_2^{(1)} - 3\left(\frac{1}{t_1} + \frac{1}{t_2}\right)\bar{f}_3^{(1)} + \frac{4}{t_2}\bar{f}_2^{(2)} - \frac{1}{t_2}\bar{f}_3^{(2)} = 0, \tag{17b}$$

$$J_x^{(N)} = -\frac{1}{t_{N-1}}\bar{f}_3^{(N-2)} + \frac{4}{t_{N-1}}\bar{f}_2^{(N-1)} - 3\left(\frac{1}{t_{N-1}} + \frac{1}{t_N}\right)\bar{f}_3^{(N-1)} - \frac{4}{t_N}\bar{f}_2^{(N)}, \tag{17c}$$

The first equation of equilibrium is given by

$$\frac{\partial \tau_{xz}^{(i)}}{\partial z} = -\sigma_{xm,m}^{(i)}(z), \quad m = 1(=x),\ 2(=y) \tag{18}$$

where repeated index m implies summation. Integration over the surface area of the triangular element and applying divergence theorem on the right side of the equation yields

$$\begin{aligned} \int\int_{S_j} \frac{\partial \tau_{xz}^{(i)}}{\partial z} dS &= -\int\int_{S_j} \sigma_{xm,m}^{(i)}(z) dS \\ &= -\int_{\Gamma_j} \sigma_{xm}^{(i)}(z) n_m d\Gamma, \quad m = 1(=x),\ 2(=y) \end{aligned} \tag{19}$$

Since for quadratic shape functions $\sigma_{xm,m}^{(i)}$ is constant with respect to x, y, integrating Eq. (18) over the area of the element and dividing by the same will not alter any thing. This step yields

$$\begin{aligned} \frac{\partial \tau_{xz}^{(i)}}{\partial z} dS &= -\frac{1}{S_j}\left[\int_{\Gamma_j} \sigma_{xm}^{(i)}(z) n_m d\Gamma\right] \\ &= -\frac{1}{S_j}\left[\sum_{k=1}^{3} \int_{\Gamma_j^{(k)}} \sigma_{xm}^{(i)}(z) n_m^{(k)} d\Gamma\right], \quad m = 1(=x),\ 2(=y) \end{aligned} \tag{20}$$

where $n_m^{(k)}$ for $m = 1\ (=x), 2\ (=y)$ and $\Gamma_j^{(k)}$ for $k = 1, \ldots, 3$ for the jth triangular element are given by Eqs. (A13) and (A14), respectively. As the in-plane stresses, $\sigma_x^{(i)}$, etc., are linear functions of x and y, one Gauss point is sufficient for exact integration on each side of the triangle. Besides, the in-plane stresses at the midpoints of the sides are exceptionally accurate (Barlow points). Finally, the jump in $\frac{\partial \tau_{xz}(z)}{\partial z}$ at the $(i+1)$th interface can now be computed as follows:

$$\begin{aligned} J_x^{(i+1)} &= \frac{\partial \tau_{xz}^{(i+1)}(0)}{\partial z} - \frac{\partial \tau_{xz}^{(i)}(t_i)}{\partial z} \\ &= -\frac{1}{S_j}\Big[\Big\{\sigma_x^{(i+1)}(0)\big|_{Node2} y_1 - \tau_{xy}^{(i+1)}(0)\Big|_{Node2} x_1 \\ &\quad + \sigma_x^{(i+1)}(0)\big|_{Node4}(y_2 - y_1) - \tau_{xy}^{(i+1)}(0)\Big|_{Node4}(x_2 - x_1) \\ &\quad - \sigma_x^{(i+1)}(0)\big|_{Node6} y_2 + \tau_{xy}^{(i+1)}(0)\Big|_{Node6} x_2\Big\} \\ &\quad - \Big\{\sigma_x^{(i)}(t_i)\big|_{Node2} y_1 - \tau_{xy}^{(i)}(t_i)\big|_{Node2} x_1 \\ &\quad + \sigma_x^{(i)}(t_i)\big|_{Node4}(y_2 - y_1) - \tau_{xy}^{(i)}(t_i)\Big|_{Node4}(x_2 - x_1) \\ &\quad - \sigma_x^{(i)}(t_i)\big|_{Node6} y_2 + \tau_{xy}^{(i)}(t_i)\Big|_{Node6} x_2\Big\}\Big], \quad \text{for } i = 1, \ldots, N-1 \end{aligned} \tag{21}$$

where $J_x^{(i+1)}$, $i = 1, \ldots, N-1$, is given by Eq. (17). Eqs. (12), (13), (15) and the combination of Eqs. (17) and (21) determine the $3N$ unknown parameters required for describing the $\tau_{xz}(z)$ distribution through the thickness of the N-layer laminated anisotropic plate under investigation. Following an identical procedure and using the second equation of equilibrium, $\tau_{yz}(z)$ distribution through the laminate thickness can be determined. $\tau_{rz}(z)$ and $\tau_{\theta z}(z)$ can obtained by usual coordinate transformation.

4. Location of exceptional points for the interlaminar shear stresses

The existence and location of special points, where the interlaminar (transverse) shear stresses are exceptionally accurate, has been explained from a physical as well as rigorous mathematical point of view by Chaudhuri and Seide [13]. They have concluded that the centroid of the quadratic triangular element is the point of exceptional accuracy for the interlaminar shear stresses. Mathematically speaking, since the interlaminar shear stresses, $\tau_{xz}(z)$ and $\tau_{yz}(z)$, use equilibrium equations in computing jumps at the layer-interfaces and hence involve the second derivatives of displacements with respect to x and y, these stresses are in error at a typical point by $O(h^{k-2})$ and on the average by $O(h^{k-1})$ for displacement functions $u^h \in S^h$ of degree $k-1$ (see Strang and Fix [29] for the notation used here). These errors must alternate in sign, and there must exist exceptional points for the interlaminar shear stresses, which are the loci of centroids of the triangular element interfaces.

5. Numerical results and discussion

The primary focus of the present study is on the determination of interlaminar (or transverse) shear stresses in the vicinity of a symmetrically (with respect to the middle surface) located internal (or embedded) part-through circular cylindrical hole in a symmetrically laminated cross-ply plate. An unsymmetrically located internal part-through hole will introduce bending-stretching coupling even in a homogeneous isotropic or symmetrically laminated plate. The present finite element formulation has been implemented in a FORTRAN code.

5.1. A rectangular three-layer cross-ply plate weakened by an internal part-through circular cylindrical hole under all-round uniform tension

The plate is as shown in Fig. 2. It has three distinct layers [90°/0°/90°], the middle layer having the same thickness as that of the internal part-through circular cylindrical hole. The layers are stacked symmetrically with respect to the middle surface. $\bar{\theta}_i = 0°$ denotes fibers in the ith layer being laid up parallel to x-axis. The following geometric parameters are selected:

$a = 50.8$ cm (20 in.), $b = 35.56$ cm (14 in.), $t = 0.762$ cm (0.3 in.), $r_0 = 5.08$ cm (2 in.), $h = 0.508$ cm (0.2 in.). The orthotropic lamina elastic properties are as follows:

$$E_{11} = 275.8\ \text{GPa (40 Msi)},\quad E_{22} = 6.895\ \text{GPa (1 Msi)},$$
$$G_{12} = G_{12} = G_{23} = 3.4475\ \text{GPa (0.5 Msi)},$$
$$\nu_{12} = \nu_{13} = 0.25,\quad \nu_{23} = 0.25.$$

E_{11} and E_{22} represent Young's moduli in the direction of the fibers and transverse to the fibers, respectively, while G_{12} denotes the in-plane shear modulus. G_{13} and G_{23} represent the transverse shear moduli in the planes parallel and normal to the fiber direction, respectively. ν_{12} denotes the major Poisson's ratio in the plane of the lamina, while ν_{13} and ν_{23} represent major Poisson's ratios in the transverse planes parallel and normal to the fiber direction, respectively.

The plate is subjected to all-round tension, $q = 689.5$ kPa (100 psi). Symmetry condition permits us to model a quarter of the plate in the x–y plane and half the thickness (Fig. 3). Symmetry with respect to the middle surface along with the assumption of transverse inextensibility also produces vanishing transverse displacements at all the nodes. The in-plane displacement symmetry conditions give rise to vanishing y-direction displacement along the x-axis (line OAB) and vanishing x-direction displacement along the y-axis (line OCD) for the nodes lying on the bottom surface and the layer-interface. For the nodes lying on the middle surface, the above symmetry conditions become vanishing y-direction displacement along the line AB and vanishing x-direction displacement along the line CD, with the circular boundary of the internal part-through hole remaining traction free. Uniform tension is applied along the lines BE and DE.

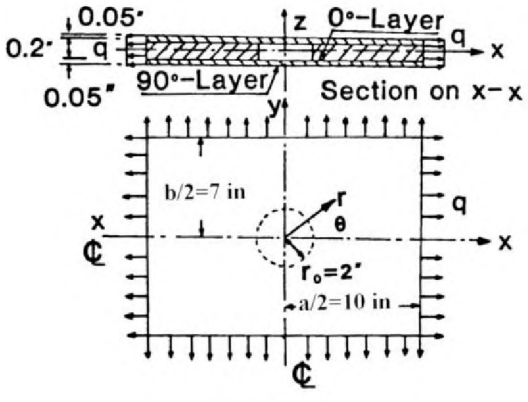

Fig. 2. Rectangular isotropic plate weakened by an internal part-through circular cylindrical hole under all-round tension.

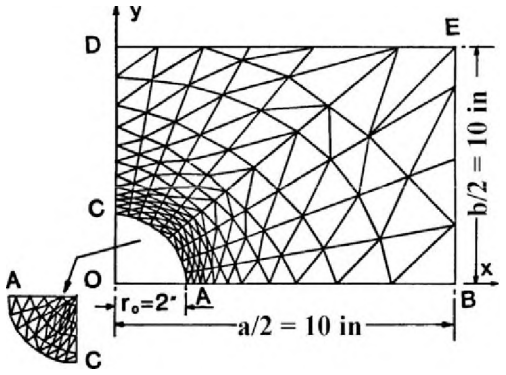

Fig. 3. Finite element model for a rectangular plate weakened by an internal part-through circular cylindrical hole.

The finite element results presented for computation of interlaminar (transverse) shear stresses using the equilibrium method have been obtained first by using quintic order of integration (full integration), and later verified by using the quadratic order or reduced integration. The interlaminar shear stresses computed by the present equilibrium/compatibility method, have been obtained by using the reduced integration alone.

Figs. 4 and 5 present variation of the mid-surface interlaminar (transverse) shear stresses, $\bar{\tau}^*_{rz} = 100\tau^{(2)}_{rz}(t_2/2)/q$ and $\bar{\tau}^*_{\theta z} = 100\tau^{(2)}_{\theta z}(t_2/2)/q$, computed at the centroids of the triangular elements adjacent to the boundary of the internal part-through circular hole ($r = 5.23$ cm = 2.067 in.), with respect to θ. The present solutions feature a nearly constant interlaminar shear stress variation in regards to the angular position, while their equilibrium counterparts show a different trend, primarily as a result oscillations. As has been observed in the case of an internal part-through circular [16] or elliptical [17] hole weakening a homogeneous isotropic plate, the results for interlaminar or transverse shear stresses computed using the equilibrium method are in serious errors. However, in comparison to their counterparts for the homogeneous isotropic case, the interlaminar (or transverse) shear stresses computed using the equilibrium method are characterized by much larger oscillations as compared to those computed using the present equilibrium/compatibility method, and this is particularly so near $\theta \sim 90°$. The extremely large errors in the interlaminar shear stresses vs. θ curves, in the neighborhood of the bi-layer interface

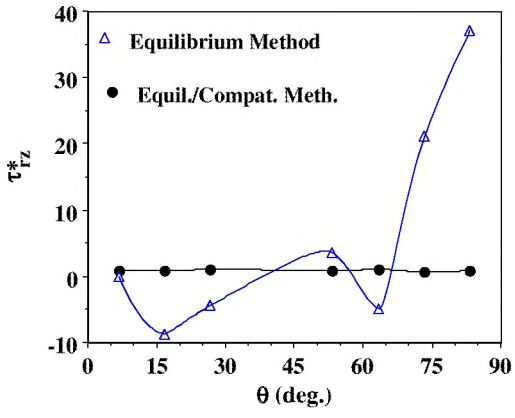

Fig. 4. Variation of the normalized transverse shear stress, τ_{rz}, around the circumference of an internal part-through circular cylindrical hole ($r = 5.23$ cm = 2.067 in.).

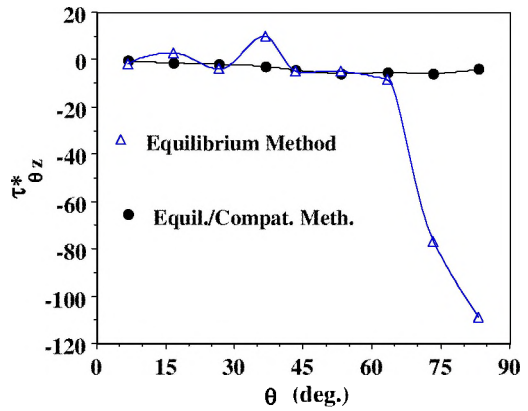

Fig. 5. Variation of the normalized transverse shear stress, $\tau_{\theta z}$, around the circumference of an internal part-through circular cylindrical hole ($r = 5.23$ cm = 2.067 in.).

circumferential re-entrant corner line of the internal part-through circular hole, in the range, $70^\circ < \theta \bullet 90^\circ$, can be attributed to the stronger influence and interaction of the free edge stress singularity at the boundary, $y = b/2$, compared to that of the edge, $x = a/2$.

It may be recalled in this connection that for a cross-ply laminate compromised by the presence of an embedded part-through hole in the middle layer, in addition to the near-field stress singularity at the circumferential line of intersection of the part-though hole with the material of the middle layer in the form of a circumferential bi-layer interface re-entrant corner, there is a far-field free-edge stress singularity at the bi-layer interface at each of the plate boundaries, $x = a/2$, and $y = b/2$. These two types (i.e., far-field and near-field) of stress singularities interact rather strongly so that the effect of the internal part-through hole never dies down at the plate boundary [7,8], and St. Venant's principle does not hold in this situation [18]. This is unlike what has been shown for the homogeneous isotropic plate weakened by an identical part-through hole [6,8].

Fig. 6(a) and (b) show variation of $\tau_{rz}^{(\tilde{l})}(z)$ and $\tau_{\theta z}^{(\tilde{l})}(z)$ through the thickness at $r = 5.23$ cm (2.067 in.), $\theta = 83.333^\circ$. As has been stated earlier, and also can be seen from Fig. 6, the transverse shear stress distribution through the thickness predicted by the equilibrium method is in serious error. Since the layer-material is homogeneous, $\tau_{rz}^{(\tilde{l})}$ vs. z curve cannot have a "corner" within a layer, because that would imply jumps (or discontinuities) in the stresses, $\sigma_r^{(\tilde{l})}(z)$ and $\tau_{r\theta}^{(\tilde{l})}(z)$, which, in turn, would imply jumps in strains, $\varepsilon_r^{(\tilde{l})}(z)$ and $\gamma_{r\theta}^{(\tilde{l})}(z)$, and consequently discontinuities in in-plane displacements at that particular z, i.e., the compatibility conditions are violated [16,17]. The apparent reason behind this lack of accuracy in the result computed by the equilibrium method is that there is only one integration constant, which cannot make the computed transverse shear stress vanish on both the bottom and top surfaces of plate, unless symmetry with respect to the middle surface is invoked [16,17]. The error in $\frac{\partial \sigma_z^{(\tilde{l})}(z)}{\partial x} + \frac{\partial \tau_{xy}^{(\tilde{l})}(z)}{\partial y}$ computed by the finite element method is "body force" like (constant through thickness in uniform stretching problems), and is of the order of $\frac{\partial \tau_{xz}^{(\tilde{l})}(z)}{\partial z}$. When $\tau_{xz}^{(\tilde{l})}(z)$ is computed by the equilibrium method by integrating the first equation of equilibrium through thickness, this error shows up as a straight line. In the case of a symmetrically (with respect to the middle surface) placed internal part-through circular cylindrical hole weakening a symmetrically laminated cross-ply plate subjected to uniform stretching, if $\tau_{xz}^{(\tilde{l})}(z)$ through half the thickness is computed by using the equilibrium method, and the same through the other half is obtained by using symmetry, this would result in the formation of a "corner" in the curve at the mid-surface, which cannot be acceptable because of the violation of the compatibility condition at the mid-surface of the plate in the immediate neighborhood of the bi-layer interface circumferential re-entrant corner line.

It is worthwhile to note from Fig. 4 of Chaudhuri [7] that $\sigma_x^{(\tilde{l})}(z)$ at the bi-layer interface (circumferential re-entrant corner line) experiences a jump at the circumference of the internal part-through circular cylindrical hole, and that the maximum stress occurs at this corner. The slope of the above curve (i.e., $\sigma_{x,x}^{(\tilde{l})}(z)$) at the bi-layer interface circumferential re-entrant corner is approximately $\tan(\pi/2) = \infty$, which, when substituted into the equilibrium equations, will yield singular transverse stresses, $\tau_{xz}^{(\tilde{l})}(z)$ and $\sigma_z^{(\tilde{l})}(z)$, in that neighborhood. Fig. 7 displays the state of stress in a 270° bi-material wedge shaped plane section normal to the bi-layer interface circumferential line of intersection of the boundary wall of the internal part-through circular cylindrical hole with its ceiling or floor (locus of point A or A' in Fig. 1). The stresses, $\sigma_R^{(\tilde{l})}$, $\sigma_\phi^{(\tilde{l})}$, $\tau_{R\phi}^{(\tilde{l})}$ and $\sigma_\theta^{(\tilde{l})}$, are singular in the vicinity of the bi-layer interface circumferential re-entrant corner line of the internal part-through circular cylindrical hole [9,19]. This translates into rendering $\sigma_r^{(\tilde{l})}$, $\tau_{rz}^{(\tilde{l})}$, $\sigma_z^{(\tilde{l})}$ and $\sigma_\theta^{(\tilde{l})}$ singular in that neighborhood. The stress field varies as $R^{-\lambda}$, $0 < \lambda < 1$, in the vicinity of the bi-layer interface circumferential corner line of the part-through hole. In the presence of a stress singularity of this kind, the stress gradients are also significantly large, which combined with the constant (through the thickness) term causes the above mentioned "body force" like error upon integration with respect to z, when the equilibrium method is used. This implies that the artificial "corner" (see

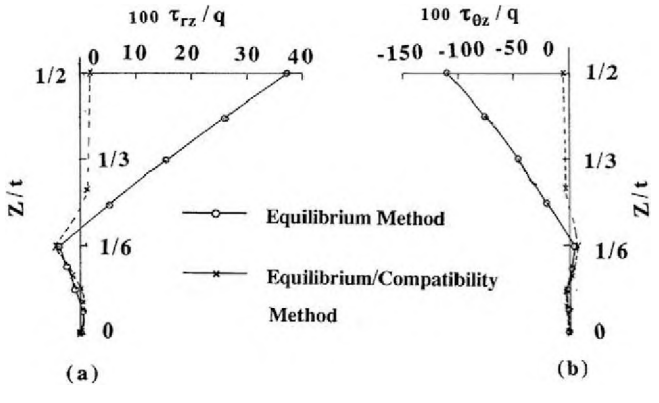

Fig. 6. Through-thickness variation of normalized transverse shear stress: (a) $100\tau_{rz}/q$ and (b) $100\tau_{\theta z}/q$ in the vicinity of an internal part-through circular cylindrical hole ($r = 5.23$ cm (2.067 in.), $\theta = 83.333^\circ$).

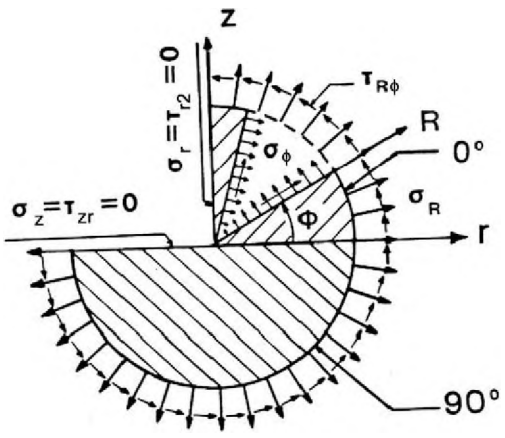

Fig. 7. Stresses on a plane 270°-wedge radial section of a laminated plate in the neighborhood of an internal part-through circular cylindrical hole.

Fig. 6) will appear whenever in-plane stress gradients do not vanish at the mid-surface of the plate, and consequently the equilibrium method will fail to deliver accurate results for the interlaminar shear stresses.

The above-mentioned "corner" and the associated "body force" like error can be eliminated by using the present method as can be seen from Fig. 6, because of its satisfaction of the bi-layer interface compatibility condition, given by Eq. (21), in the form of condition (iv) of Section 3. In this connection, it may be remarked that the accuracy (or lack thereof) of the equilibrium method is a good indicator of the accuracy of the computed intra-laminar (in-plane) stresses (strictly speaking stress gradients), since this method depends on equilibrium of these stresses. This is in line with the fact that the computed in-plane stresses including $\sigma_{\theta}^{(i)}$ computed at the edge of the hole at or near $\theta \sim 90^{\circ}$ may be in some error. As has been discussed earlier [16,17], the subparametric version of the assumed quadratic displacement triangular element cannot accurately predict the stresses in the elements located inside the "boundary layer" zone.

A comparison of the computed through-thickness distribution of the interlaminar shear stress, $\tau_{rz}^{(i)}$, in the vicinity of an internal part-through circular cylindrical hole, shown in Fig. 6(a), with its counterpart for a homogeneous plate, shown in Fig. 4 of Chaudhuri [16], reveals that the present interlaminar shear stress, $\tau_{rz}^{(i)}$, can vary from negative to positive through the thickness of a cross-ply plate in the neighborhood of the above-mentioned kind of stress singularity, while its homogeneous isotropic counterpart is always positive, other factors remaining unaltered. Furthermore, the interlaminar shear stress, $\tau_{rz}^{(i)}$, is, in the present case, much smaller in magnitude than its counterpart for a homogeneous isotropic plate.

6. Summary and conclusions

The equilibrium/compatibility method, which is a semi-analytical post-processing method, is employed for computation of hitherto unavailable through-thickness variation of interlaminar (transverse) shear stresses in the vicinity of the bi-layer interface circumferential re-entrant corner line of an internal part-through circular cylindrical hole weakening an edge-loaded laminated composite plate. A C^{o}-type triangular composite plate element, based on the assumptions of transverse inextensibility and layer-wise constant shear-angle theory (LCST), is utilized to first compute the in-plane stresses and layer-wise through-thickness average interlaminar shear stresses, which serve as the starting point for computation of through-thickness distribution of interlaminar shear stresses in the vicinity of the bi-layer interface circumferential re-entrant corner line of the part-through hole.

The present investigation re-affirms, to a rather extreme degree, the conclusion reached earlier in the case of its homogeneous counterpart [16] in regards to the accuracy (or lack thereof) of the stresses computed using the conventional (assumed displacement potential energy based) finite element analysis and computed FEM-based post-processing analysis results for interlaminar shear stresses in the vicinity of a stress singularity, such as the bi-layer interface circumferential corner line of an internal circular cylindrical hole. Eq. (21) constitutes the required layer-interface compatibility equation, when a weak or integral form of solution (in Sobolev space, H^{1}) is sought with convergence in the L_2 norm [16,17]. This equation is the counterpart of the compatibility (differential) equation (see last of Eq. (4), p. 101, Fung [30]) when strong or differential form of solution is sought with convergence in the sup norm.

This problem is not restricted to the FEM alone, but pervades all over discrete integral equations based methods, such as the FFT (fast Fourier transform) or BIE (boundary integral equations). The following important conclusions are drawn from the numerical results of the present finite element based post-processing analysis:

(i) The present solutions feature a nearly constant interlaminar shear stress variation in regards to the angular position, while their equilibrium counterparts show a different trend, primarily as a result oscillations discussed below in item (iii).

(ii) The transverse shear stress, $\tau_{rz}^{(i)}$, computed using the conventional equilibrium method is in serious error in the presence of the stress singularity at the bi-layer interface circumferential re-entrant corner line of an internal part-through circular cylindrical hole. This is because $\tau_{rz}^{(i)}$ is singular. This error is "body force" like, and is due to the violation of the compatibility equation in the presence of stress singularity.

(iii) In comparison to their counterparts for the homogeneous isotropic case, the interlaminar (or transverse) shear stresses computed using the equilibrium method are characterized by much larger oscillations (errors) as compared to those computed using the present equilibrium/compatibility method, and this is particularly so near $\theta \sim 90^{\circ}$.

(iv) The extremely large errors in the interlaminar shear stresses (computed using the equilibrium method) vs. θ curves, in the neighborhood of the bi-layer interface circumferential re-entrant corner line of the internal part-through circular cylindrical hole, in the range, $70^{\circ} < \theta \bullet 90^{\circ}$, can be attributed to the stronger influence and interaction of the free edge stress singularity at the boundary, $y = b/2$, compared to that of the edge, $x = a/2$.

(v) For a cross-ply laminate compromised by the presence of an embedded part-through hole in the middle layer, in addition to the near-field singularity at the circumferential line of intersection of the part-though hole with the material of the middle layer in the form of a circumferential bi-layer interface re-entrant corner, there is a far-field free-edge stress singularity at the bi-layer interface at the plate boundaries, $x = a/2$, and $y = b/2$. These two types of stress singularities (i.e., near-field and far-field) interact so that the effect of the internal part-through hole never dies down at the plate boundary, and St. Venant's principle does not hold in this situation. This is unlike what has been shown for the homogeneous isotropic plate weakened by an otherwise identical part-through hole.

(vi) The above error can be eliminated by using the present method because of its satisfaction of layer-interface compatibility condition in the vicinity of the circumferential re-entrant corner line singularity arising out of the internal part-through hole.

(vii) A comparison of the computed through-thickness distribution of the interlaminar shear stress, $\tau_{rz}^{(i)}$, in the vicinity of an internal part-through circular cylindrical hole with its counterpart for a homogeneous plate reveals that the present interlaminar shear stress can vary from negative to positive through the thickness of a cross-ply plate in the neighborhood of the above-mentioned kind of stress singularity, while its homogeneous isotropic counterpart is always positive, other factors remaining unaltered. Furthermore, the interlaminar shear stress, $\tau_{rz}^{(i)}$, is, in the present case, much smaller in magnitude than its counterpart for a homogeneous isotropic plate.

Extension of the present approach to the variation of transverse normal stress through thickness is currently under way, and will be reported in a future paper. In addition, the present analysis is currently being extended to the case of an internal elliptical hole weakening a cylindrical panel [31], and will be reported in the future.

Appendix A

$[A^{(i)}]$, $i = 1,\ldots,N$, referred to in Eq. (8) is given by

$$[A^{(i)}] = \begin{bmatrix} [A_b^{(i)}] & [A_t^{(i)}] & [0] \\ [0] & [0] & [A_s^{(i)}] \end{bmatrix}, \tag{A1}$$

where

$$[A_b^{(i)}] = \begin{bmatrix} 1-\frac{z}{t_i} & 0 & 0 \\ 0 & 1-\frac{z}{t_i} & 0 \\ 0 & 0 & 1-\frac{z}{t_i} \end{bmatrix}, \tag{A2a}$$

$$[A_t^{(i)}] = \begin{bmatrix} \frac{z}{t_i} & 0 & 0 \\ 0 & \frac{z}{t_i} & 0 \\ 0 & 0 & \frac{z}{t_i} \end{bmatrix}, \tag{A2b}$$

and

$$[A_s^{(i)}] = \begin{bmatrix} 1 & 0 \\ 0 & 1 \end{bmatrix}. \tag{A2c}$$

$[C^{(i)}]$, $i = 1,\ldots,N$, for an anisotropic lamina can be expressed in terms of its counterpart for a 0°-lamina, $[\overline{C}^{(i)}]$, as follows:

$$[C^{(i)}] = [\overline{T}]^T\ [\overline{C}^{(i)}]\ [\overline{T}], \tag{A3}$$

where

$$[\overline{C}^{(i)}] = \begin{bmatrix} [\overline{C}_l^{(i)}] & [0] \\ [0] & [\overline{C}_G^{(i)}] \end{bmatrix}, \tag{A4}$$

with

$$[\overline{C}_l^{(i)}] = \begin{bmatrix} \bar{c}_{11}^{(i)} & \bar{c}_{12}^{(i)} & 0 \\ & \bar{c}_{22}^{(i)} & 0 \\ Symm & & \bar{c}_{66}^{(i)} \end{bmatrix}, \tag{A5a}$$

and

$$[\overline{C}_G^{(i)}] = \begin{bmatrix} \bar{c}_{44}^{(i)} & 0 \\ Symm & \bar{c}_{55}^{(i)} \end{bmatrix}, \tag{A5b}$$

while

$$[\overline{T}] = \begin{bmatrix} \cos^2\bar{\theta}_i & \sin^2\bar{\theta}_i & \frac{1}{2}\sin(2\bar{\theta}_i) & 0 & 0 \\ \sin^2\bar{\theta}_i & \cos^2\bar{\theta}_i & -\frac{1}{2}\sin(2\bar{\theta}_i) & 0 & 0 \\ -\sin(2\bar{\theta}_i) & \sin(2\bar{\theta}_i) & \cos(2\bar{\theta}_i) & 0 & 0 \\ 0 & 0 & 0 & \cos\bar{\theta}_i & \sin\bar{\theta}_i \\ 0 & 0 & 0 & -\sin\bar{\theta}_i & \cos\bar{\theta}_i \end{bmatrix}. \tag{A6}$$

$\left\{d_j^{(i)}\right\}$, as referred to in Eq. (8), is given as follows:

$$\left\{d_j^{(i)}\right\}^T = \left\{\bar{u}_1^{(i)}, \bar{v}_1^{(i)}, \ldots, \bar{u}_6^{(i)}, \bar{v}_6^{(i)}, \bar{u}_1^{(i+1)}, \bar{v}_1^{(i+1)}, \ldots, \bar{u}_6^{(i+1)}, \bar{v}_6^{(i+1)}, w_1, \ldots, w_6\right\}. \tag{A7}$$

$\left[B_j^{(i)}\right]$, as referred to in Eq. (8), is given by

$$\left[B_j^{(i)}\right] = \begin{bmatrix} [R] & [0] & [0] \\ [0] & [R] & [0] \\ [M^{(i)}] & [N^{(i)}] & [T] \end{bmatrix}, \tag{A8}$$

whose submatrices are given as follows:

$$[R] = [[R_1]\ \ldots\ [R_k]\ \ldots\ [R_6]\ ],\quad k = 1,\ldots,6, \tag{A9a}$$

in which

$$[R_k] = \begin{bmatrix} \phi_{k,1} & 0 \\ 0 & \phi_{k,2} \\ \phi_{k,2} & \phi_{k,1} \end{bmatrix}, \tag{A9b}$$

$$[T] = [[T_1]\ \ldots\ [T_k]\ \ldots\ [T_6]],\ k = 1,\ldots,6, \tag{A10a}$$

$$[T_k] = \begin{bmatrix} \phi_{k,1} & \\ & \\ & \phi_{k,2} \end{bmatrix}, \tag{A10b}$$

$$[N^{(i)}] = \left[\left[N_1^{(i)}\right]\ \ldots\ \left[N_k^{(i)}\right]\ \ldots\ \left[N_6^{(i)}\right]\right],\quad k = 1,\ldots,6;\ i = 1,\ldots,N, \tag{A11a}$$

with

$$\left[N_k^{(i)}\right] = \begin{bmatrix} \frac{\phi_k}{t_i} & 0 \\ 0 & \frac{\phi_k}{t_i} \end{bmatrix}, \tag{A11b}$$

while

$$[M^{(i)}] = -[N^{(i)}],\ i = 1,\ldots,N. \tag{A12}$$

ϕ_k, $k = 1,\ldots,6$, referred to above in Eqs. (A9), (A10) and (A11), represents the shape function for the kth node of a triangular element interface, and is given by

$$\{\phi\}^T = \{\zeta_1, (2\zeta_1 - 1),\ 4\zeta_1\zeta_2,\ \zeta_2(2\zeta_2 - 1),\ 4\zeta_2\zeta_3,\ \zeta_3(2\zeta_3 - 1),\ 4\zeta_3\zeta_1\}, \tag{A13}$$

where ζ_k, $k = 1, 2, 3$ represents area coordinates.

$n_m^{(k)}$, $m = 1$ (=x), 2 (=y), and $k = 1,\ldots,3$, referred to in Eq. (20) and Fig. 8, is defined as follows:

$$n_1^{(1)} = \frac{y_1}{\Gamma_1^{(j)}},\qquad n_2^{(1)} = -\frac{x_1}{\Gamma_1^{(j)}}, \tag{A14a, b}$$

$$n_1^{(2)} = \frac{y_2 - y_1}{\Gamma_2^{(j)}},\qquad n_2^{(2)} = -\frac{x_2 - x_1}{\Gamma_2^{(j)}}, \tag{A14c, d}$$

$$n_1^{(3)} = -\frac{y_2}{\Gamma_3^{(j)}},\qquad n_2^{(3)} = \frac{x_2}{\Gamma_3^{(j)}}, \tag{A14e, f}$$

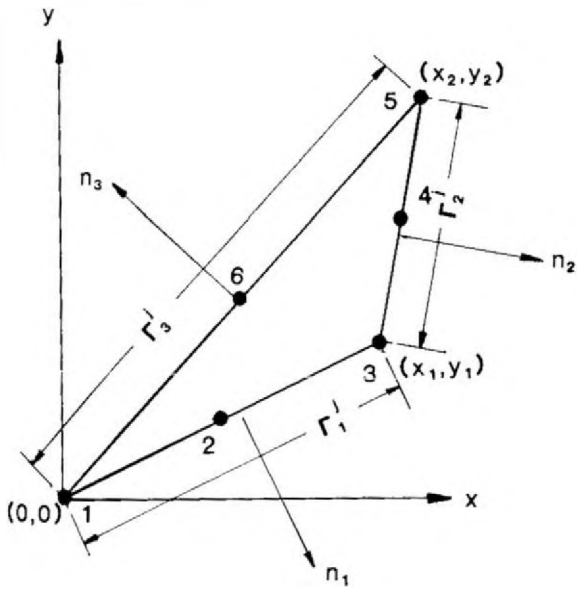

Fig. 8. jth triangular element interface.

in which

$$\Gamma_1^{(j)} = \left(x_1^2 + y_1^2\right)^{1/2},$$
$$\Gamma_2^{(j)} = \left[(x_2 - x_1)^2 + (y_2 - y_1)^2\right]^{1/2},$$
$$\Gamma_3^{(j)} = \left(x_2^2 + y_2^2\right)^{1/2}. \qquad \text{(A15a,b,c)}$$

References

[1] Barker RM, Dana JR, Pryor CW. Stress concentration near holes in laminates. J Eng Mech Div ASCE 1974;100(EM3):477–88.
[2] Rybicki EF, Schmueser DW. Effect of stacking sequence and lay-up angle on free edge stresses around a hole in a laminated plate under tension. J Compos Mater 1978;12:300–13.
[3] Delale F. Stress analysis of multilayered plates around circular holes. Int J Eng Sci 1984;22:57–75.
[4] Chaudhuri RA, Seide P. Triangular element for analysis of perforated plates under inplane and transverse loads. Comput Struct 1986;24:87–95.
[5] Chaudhuri RA. An eigenfunction expansion solution for three-dimensional stress field in the vicinity of the circumferential line of intersection of a bimaterial interface and a hole. Int J Fract 2004;129:361–84.
[6] Chaudhuri RA, Seide P. Triangular element for analysis of a stretched plate weakened by a part-through hole. Comput Struct 1986;24:97–105.
[7] Chaudhuri RA. Stress concentration around a part-through hole weakening a laminated plate. Comput Struct 1987;25:601–9.
[8] Chaudhuri RA. Weakening effects of internal part-through elliptic holes on homogeneous and laminated composite plates. Compos Struct 2007;81:362–73.
[9] Chaudhuri RA. Three-dimensional asymptotic stress field in the vicinity of the line of intersection of a circular cylindrical through/part-through open/rigidly plugged hole and a plate. Int J Fract 2003;122:65–88.
[10] Chaudhuri RA. An equilibrium method for prediction of transverse shear stresses in a thick laminated plate. Comput Struct 1986;23:139–46.
[11] Engblom JJ, Ochoa OO. Finite element formulation including interlaminar stress calculations. Comput Struct 1986;23:231–49.
[12] Chaudhuri RA, Seide P. An approximate method for prediction of transverse shear stresses in a laminated shell. Int J Solids Struct 1987;23:1145–61.
[13] Chaudhuri RA, Seide P. An approximate semi-analytical method for prediction of interlaminar shear stresses in an arbitrarily laminated thick plate. Comput Struct 1987;25:627–36.
[14] Chaudhuri RA. A semi-analytical approach for prediction of interlaminar shear stresses in laminated general shells. Int J Solids Struct 1990;26:499–510.
[15] Chaudhuri RA, Balaraman K, Kunukkasseril VX. Admissible boundary conditions and solutions to internally pressurized thin arbitrarily laminated cylindrical shell boundary-value problems. Compos Struct 2008;86:385–400.
[16] Chaudhuri RA. Computation of transverse shear stresses in the vicinity of the circumferential re-entrant corner line of an internal part-through hole weakening an edge-loaded plate. Compos Struct 2009;89:315–20.
[17] Chaudhuri RA. Transverse shear stress distribution through thickness near an internal part-through elliptical hole in a stretched plate. Compos Struct, in press.doi:10.1016/j.compstruct.2009.08.021.
[18] Chaudhuri RA, Xie M. A tale of two saints: St. Venant and "St. Nick" – does St. Venant's principle apply to bi-material straight edge and wedge singularity problems? Compos Sci Technol 2000;60:2503–15.
[19] Chaudhuri RA, Chiu SJ. Three-dimensional asymptotic stress field at the front of an unsymmetric bimaterial wedge associated with matrix cracking or fiber break. Compos Struct 2007;78:254–63.
[20] Pipes RB, Pagano NJ. Interlaminar stresses in composite laminates under uniform axial extension. J Compos Mater 1970;4:538–48.
[21] Wang SS, Choi I. Boundary-layer effects in composite laminates: part 1 – free-edge stress singularities. ASME J Appl Mech 1982;49:541–8.
[22] Chaudhuri RA, Xie M. Free-edge stress singularity in a bimaterial laminate. Compos Struct 1998;40:129–36.
[23] Chaudhuri RA, Chiu SJ. Three-dimensional asymptotic stress field in the vicinity of an adhesively bonded scarf joint interface. Compos Struct 2009;89:475–83.
[24] Chaudhuri RA, Seide P. Triangular finite element for analysis of thick laminated plates. Int J Numer Methods Eng 1987;24:1203–24.
[25] Chaudhuri RA. Analysis of laminated shear-flexible angle-ply plates. Compos Struct 2005;67:71–84.
[26] Seide P, Chaudhuri RA. Triangular finite element for analysis of thick laminated shells. Int J Numer Methods Eng 1987;24:1563–79.
[27] Chaudhuri RA. A simple and efficient plate bending element. Comput Struct 1987;25:817–24.
[28] Chaudhuri RA. A degenerate triangular shell element with constant cross-sectional warping. Comput Struct 1988;28:315–25.
[29] Strang G, Fix G. The finite element method. 3rd ed. Englewood Cliffs, NJ: Prentice-Hall; 1973.
[30] Fung YC. Foundations of solid mechanics. Englewood Cliffs, NJ: Prentice-Hall; 1965.
[31] Chaudhuri RA. A new three-dimensional shell theory in general (Non-Lines-of-Curvature) Coordinates for analysis of curved panels weakened by through/part-through holes. Compos Struct 2009;89:321–32.